Simulation of a complete reflected shock tunnel showing a vortex mechanism for flow contamination.

Richard J. Goozée
Department of Mechanical Engineering,
The University of Queensland, Queensland, Australia
(presently at WBM Pty Ltd, Brisbane)
rjgoozee@wbmpl.com.au

Peter A. Jacobs
Department of Mechanical Engineering,
The University of Queensland, Queensland, Australia
peterj@mech.uq.edu.au

David R. Buttsworth
Faculty of Engineering and Surveying,
The University of Southern Queensland, Queensland, Australia
buttswod@usq.edu.au

Communicated by [see published version]

Received [see published version]

Abstract. Simulations of a complete reflected shock tunnel facility have been performed with the aim of providing a better understanding of the flow through these facilities. In particular, the analysis is focused on the premature contamination of the test flow with the driver gas. The axisymmetric simulations model the full geometry of the shock tunnel and incorporate an iris-based model of the primary diaphragm rupture mechanics, an ideal secondary diaphragm and account for turbulence in the shock tube boundary layer with the Baldwin-Lomax eddy viscosity model. Two operating conditions were examined: one resulting in an over-tailored mode of operation and the other resulting in approximately tailored operation. The accuracy of the simulations is assessed through comparison with experimental measurements of static pressure, pitot pressure and stagnation temperature. It is shown that the widely-accepted driver gas contamination mechanism in which driver gas 'jets' along the walls through action of the bifurcated foot of the reflected shock, does not directly transport the driver gas to the nozzle at these conditions. Instead, driver gas laden vortices are generated by the bifurcated reflected shock. These vortices prevent jetting of the driver gas along the walls and convect driver gas away from the shock tube wall and downstream into the nozzle. Additional vorticity generated by the interaction of the reflected shock and the contact surface enhances the process in the over-tailored case. However, the basic mechanism appears to operate in a similar way for both the over-tailored and the approximately tailored conditions.

1. Introduction

The full potential of free piston driven reflected shock tunnels in high enthalpy operation has not been reached in practice due to the premature contamination of the test flow with the driver gas (Stalker and Crane, 1978).

Over the years, various analytical and empirical models have been developed in an attempt to predict driver gas contamination (Stalker and Crane, 1978; Skinner, 1994; Paull, 1996), but they have never been successful across a range of operating conditions. Attempts at understanding driver gas contamination have been based on the mechanism first described by Mark (1957). Mark (1957) observed that the reflected shock can bifurcate as it moves upstream through the shock tube boundary layer and that the gas emerging from the two oblique shocks at the bifurcated foot can have a higher velocity than the gas that passes through the normal shock. Burtschell et al. (2001) stated that the driver gas that passes through this bifurcated region penetrates into the test gas as a jet along the tube wall to contaminate the test flow; however, this phenomenon appears to be incapable of explaining the observations of contamination in previous experimental studies (Skinner, 1994; Cardoso et al., 1997).

To improve the understanding of key shock tunnel processes such as contamination, axisymmetric numerical simulations have been used (Sharma and Wilson, 1995; Wilson, 1995; Chue and Eitelberg, 1998); however, previous axisymmetric simulations of reflected shock tunnels have generally modelled only particular parts of a facility. Typically the very end of the shock tube and the nozzle have been modelled using inflow conditions derived from empirical relations (Sharma and Wilson, 1995; Wilson, 1995). The results obtained in these simulations are heavily dependent on the assumptions associated with modelling only part of a facility. Axisymmetric simulations have also aimed specifically at modelling the interaction of the reflected shock with the boundary layer, for the purpose of interpreting its effect on flow contamination by the driver gas (Wilson, 1995; Badcock, 1992). Chue and Eitelberg (1998) noted the generation of vorticity in the driver gas interface during its interaction with the reflected shock; however, the process was not followed through its complete evolution and it was concluded that this vorticity would act to postpone contamination.

The simulations described in this paper represent a contribution beyond that of previous axisymmetric reflected shock tunnel simulations because a complete facility from the driver section to the dump tank has been simulated. This is significant because it transpires that contamination of the test gas occurs through the combination of a number of mechanisms that occur during the evolution of the flow along the length of the shock tunnel. Thus, identification of the actual contamination mechanisms is more likely to be achieved through complete tunnel simulations than by modelling parts of the facility in isolation.

The simulations are validated by comparing the temporal variation of simulated flow quantities with experimental measurements at particular locations within the shock tunnel for the two operating conditions. As with previous axisymmetric simulations (Sharma and Wilson, 1995; Wilson, 1995), experimental benchmarking is achieved using reflected shock tunnel data for relatively low enthalpy conditions to avoid the complication of thermochemical effects experienced with high enthalpy operation. Having assessed the accuracy of the simulations, results are then presented to illustrate the simulated driver gas contamination mechanisms observed for the two shock tunnel operating conditions.

2. Overview of the Simulations

The simulations described in this paper model the flow through the Drummond Tunnel, which is a relatively low enthalpy reflected shock tunnel operated within the Centre for Hypersonics at the University of Queensland (Austin et al., 1997; Craddock et al., 1998). Figure 1 illustrates the Drummond Tunnel facility and the associated instrumentation. Although the tunnel produces a relatively low enthalpy flow, it can still be used to investigate the fluid mechanics that operate in a modified form at higher enthalpies. Data from this tunnel can also be used to establish whether driver gas contamination can be predicted by numerical simulations of complete facilities. The simulations are provided with only the geometry and the initial tube filling and boundary conditions from the operation of the real facility and are run from the initiation of the rupture of the primary diaphragm.

The simulations were performed using the multi-block CFD code, MB_CNS (Jacobs, 1996),

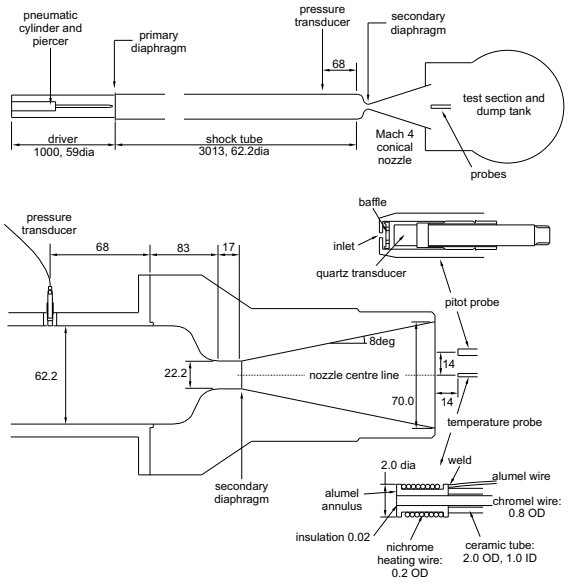

Figure 1. Illustration of the reflected shock tunnel arrangement and associated instrumentation. Dimensions are in mm.

which is based on a finite-volume formulation of the compressible Navier-Stokes equations. It has a shock-capturing capability through the use of a limited reconstruction scheme and an adaptive flux calculator that switches from AUSM (Wada and Liou, 1994) to the Equilibrium Flux Method (EFM) (Macrossan, 1989) where large velocity gradients are detected.

An axisymmetric, body-fitted mesh is used to represent the geometry of the complete facility, including the driver section, the length of the shock tube, the Mach 4 nozzle, the test section and the dump tank. The axisymmetric approach allows a good representation of the cylindrical geometry of the shock tunnel, but prevents circumferential motion or gradients. This approximation is used because it affords considerable computational savings relative to fully three dimensional modelling, but has the effect of forcing artificially high levels of coherence in vortical structures. The meshes were refined towards the walls, to resolve the boundary layer, and towards regions where the geometry of the shock tube changed.

Two refinements of the original (coarse) mesh were used for convergence studies. The number of cells across the radius of the shock tube was varied from 40 cells for the coarse mesh, to 60 cells for the medium mesh and 80 cells for the fine mesh. These three meshes consisted of a total of 80,850 to 181,980 and 323,400 cells respectively. Analysis of the simulated flow field produced with these meshes showed that there was an adequate level of convergence in the results produced with the finest mesh. The simulated results and images presented in this paper were obtained using the fine resolution mesh. Further details on the mesh refinement studies are available in Goozée (2003).

The simulation of a complete experimental test in a shock tunnel requires the simulation of high speed transient flow for a significant period of time. This means that the large mesh sizes are combined with the requirement for marching the solution over large numbers of time steps. Such large scale simulations have been made possible through the use of parallel processing supercomputing. The meshes were decomposed into 24 blocks in order to represent the geometry of the facility and to allow parallelisation of the solution.

A constant temperature of 296 K (equal to the ambient temperature) was specified at the wall boundaries because only small changes (typically less that 5 K) in surface temperature occur over the period of interest during the experiments. Since all of the gases used in the facility are modelled, there are no gas inflow or outflow boundaries in the simulation.

The peak temperatures in the stagnation region at the end of the shock tube remain below 1600 K. At these temperatures, vibrational modes of excitation of the nitrogen molecules are not yet significant. For the Helium driving Nitrogen case, the gas model assumed that the gas was a mixture of perfect gases. For the Nitrogen driving Nitrogen cases, a look-up table, based on the CEA program (Gordon and McBride, 1994; McBride and Gordon, 1996) was used.

The properties of gases composed of multiple components (or species) are modelled by solving additional equations for conservation of each of these component gases. The properties of the gas mixture in each cell can then be calculated using mass fraction weighted averages of the component gas properties.

The flow in the real facility is initiated by the rupture of an aluminium diaphragm separating the driver gas from the driven gas. In order to obtain an adequate simulation of the performance of the actual shock tunnel, it was necessary to account for the finite opening time of the primary diaphragm. The primary diaphragm was assumed

to rupture with a linear profile of opened cross-sectional area versus time that was derived from the experiments of Rothkopf and Low (1974). The radius of the opening diaphragm was increased at each time step, until the final radius (identified from measurements on spent Drummond Tunnel diaphragms) was reached.

The Drummond Tunnel also has a thin secondary diaphragm, which initially separates the test gas from the dump tank section. Following the arrival of the shock at the secondary diaphragm, the pressure rises rapidly and the diaphragm bursts within a very short period. In these simulations the secondary diaphragm is assumed to rupture instantaneously and completely when a specified pressure rise occurs at its upstream face.

The simulations initially modelled the boundary layers as laminar. These simulations significantly over-estimated the incident shock pressure. The accuracy of the simulations was improved by accounting for the effect of turbulence in the boundary layers on the shock tube wall and nozzle. The Baldwin-Lomax eddy viscosity model (Baldwin and Lomax, 1978) was used. The model is computationally inexpensive and robust; however, it is an incomplete turbulence model and requires knowledge of the flow conditions being modelled in the form of modifiable coefficients.

3. Experimental Validation

The simulations that are described in this paper reproduced the initial conditions of two sets of experiments that were performed in the Drummond Tunnel facility, one resulting in over-tailored and the other in approximately tailored operation. The initial conditions of the simulations were specified to match the initial tube filling conditions used in these experiments, as given in Table 1.

Table 1. The two filling conditions.

Driver	Shock tube	Level of tailoring
N_2	N_2	over-tailored
3.25 MPa	30.0 kPa	
He	N_2	approximately tailored
5.60 MPa	61.4 kPa	

The tube filling pressures were known from the experiments (as shown in Table 1), but it was later found that the initial temperature of the driver gas would have been somewhat higher than the ambient temperature (296 K) depending on the rate at which the driver section was filled and the delay before the experiment. Since the actual driver gas temperature immediately prior to diaphragm rupture was not measured, the initial temperature of the driver gas in the simulation was tuned within the subsequently measured limits of 303 and 313 K until the incident shock speed matched that of the experiment. The ambient temperature of 296 K was used as the initial temperature of the shock tube (driven) and dump tank gases because there was sufficient time prior to the primary diaphragm rupture to achieve thermal equilibrium.

The experiments provided sets of measured data which were used to validate the numerical simulations. Data were recorded during the experiments by a pressure transducer on the wall of the shock tube in the stagnation region near the end of the shock tube and by a pitot pressure probe that was located close to the exit plane of the Mach 4 nozzle. The arrangement of the instrumentation is shown in Figure 1. In the over-tailored case, a stagnation temperature probe (Buttsworth and Jacobs, 1998) was used to provide additional validation data. Unfortunately the stagnation temperature probe was not available for use in the approximately tailored experiments which were conducted as a separate campaign from the over-tailored experiments. Simulated data traces were also recorded at corresponding locations throughout the simulations.

Figure 2 shows a comparison between the simulated and the experimentally measured nozzle supply static pressure traces for the over-tailored case. For all of the comparisons between the simulated and experimental data presented in this paper, the time scale for both the simulated and experimental results is referenced to the arrival of the incident shock at the nozzle supply pressure transducer. The traces show that the simulation reproduces the conditions behind both the incident and reflected shocks, although there is a deviation between about 0.6 and 0.8 ms on the timescale in Figure 2. This deviation, which occurs when the bifurcated foot of the reflected shock passes over the transducer, has been noted in previous simulations of reflected shock-boundary layer interactions (Weber et al., 1995). The overall rate of pressure rise associated with the over-tailored con-

ditions (between about 1.2 and 3.0 ms) is reproduced by the simulations; however, the simulated pressure rise proceeds via wave processes that are more discrete than observed experimentally.

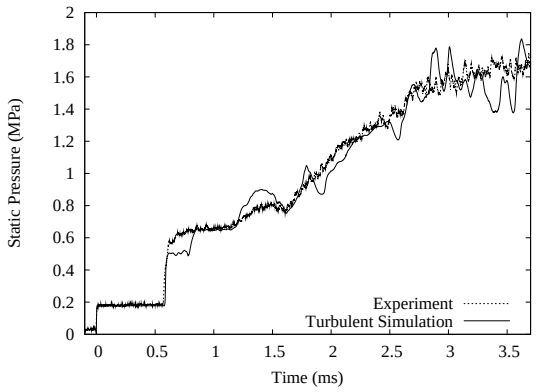

Figure 2. Comparison between the simulated (solid) and experimentally measured (dashed) nozzle supply pressure transducer traces for the over-tailored case.

Figure 3 shows a comparison between the simulated and the experimentally measured pitot pressure traces for the over-tailored case. The arrival of the nozzle startup waves occurs at approximately 0.35 ms and the test flow is not established until about 0.7 ms. The simulations accurately reproduce the test flow pitot pressure and the steady test time. The arrival time of the pressure rise associated with the over-tailoring (at about 1.55 ms on this scale) is reproduced; however, as with the nozzle supply pressure history, the over-tailoring pressure waves are more discrete in the simulation than in the real flow.

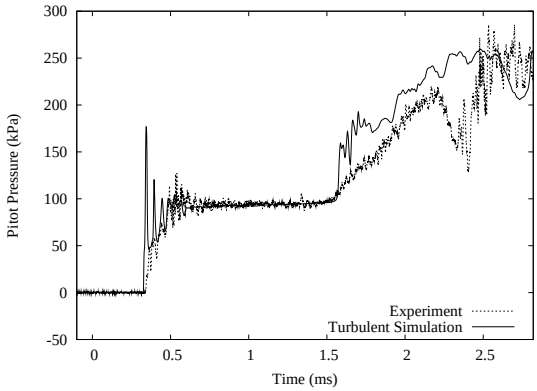

Figure 3. Comparison between the simulated (solid) and experimentally measured (dashed) test flow pitot pressure traces for the over-tailored case.

Figure 4 shows the data obtained from the stagnation temperature probe, which provides a direct indication of driver gas arriving in the test flow for the over-tailored case. This figure shows that the driver gas arrives at the stagnation temperature probe at about 2.2 ms. The simulation reproduces the arrival time of the driver gas to within approximately 0.1 ms. This result supports the assertion that the essential fluid mechanics, and in particular, the driver gas dynamics, is being modelled with sufficient accuracy. A difference of 0.1 ms amounts to a spatial error of less than 15 mm (about one quarter of the tube diameter) at the average convection velocity of the main contaminating structure in the end of the shock tube.

The dip in the experimentally measured pitot pressure (Figure 3) at about 2.2 ms is presumably associated with the arrival of the cold driver gas in the test section given the decrease in the experimental stagnation temperature data at this same time (Figure 4). The simulated pitot pressure does not exhibit such a dip, nor is one expected at this time since the nozzle exit Mach number should remain largely unchanged with the arrival of the cold gas meaning the pitot pressure should vary only with the nozzle supply pressure in this case. We suggest the dip in the experimentally measured pitot pressure is a consequence of the interaction of the transient flow and the probe (which was not simulated), and the response time of the pitot probe (see Figure 1) which is around 0.1 ms.

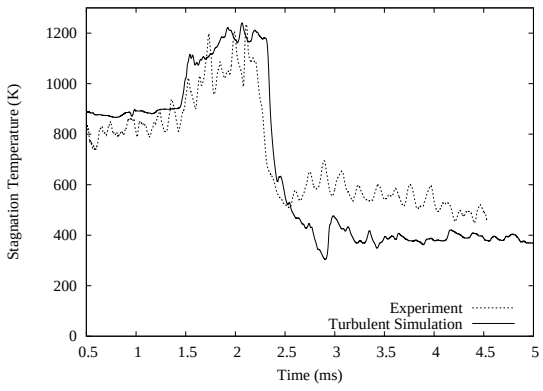

Figure 4. Comparison between the simulated (solid) and experimentally measured (dashed) nozzle exit stagnation temperature for the over-tailored case. The dip in stagnation temperature at around 2.2 ms corresponds to the arrival of driver gas in the test flow.

Figures 5 and 6 compare the simulated and the experimentally measured pressure traces for the approximately tailored case. Apart from deviations associated with the bifurcated reflected shock (between about 0.45 and 0.7 ms in Figure 5), the simulation reproduces the incident and reflected shock static pressures. The resulting test flow pitot pressure is also reproduced quite well. The test time, being defined as the duration over which approximately constant pressure conditions are produced is likewise simulated accurately. The overall decrease in pressure after 1 ms, ending the test time, is simulated with reasonable accuracy for both the nozzle supply static pressure (Figure 5) and the nozzle exit pitot pressure (Figure 6). This pressure decrease is associated with the arrival of the expansion that has reflected from the upstream end of the driver tube, rather than tailoring effects.

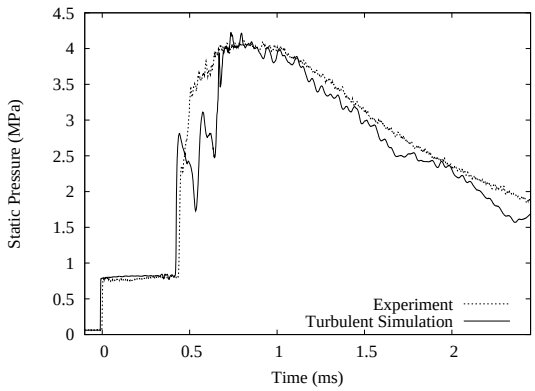

Figure 5. Comparison between the simulated (solid) and experimentally measured (dashed) nozzle supply pressure transducer traces for the approximately tailored case.

The overall pressure levels and the rates of change of pressure have been simulated with reasonable accuracy. The primary differences between the simulated and experimental results are: 1) the bifurcated foot of the reflected shock produces a simulated pressure rise via discrete structures that are not observed experimentally; and 2) the simulated disturbances following the interaction of the reflected shock with the incident contact surface (in particular, the tailoring waves in the over-tailored case) are also of a larger magnitude and more discrete nature than observed experimentally. These differences are believed to be associated with the simulation maintaining unrealistically high levels of structural coherence,

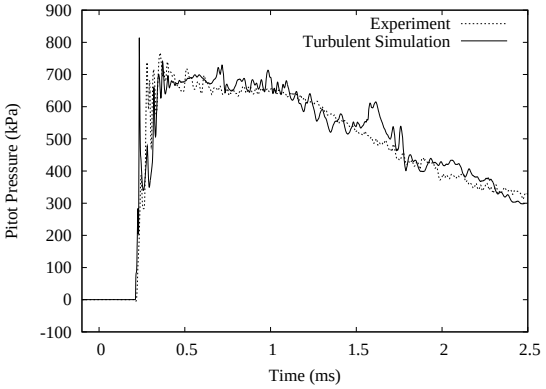

Figure 6. Comparison between the simulated (solid) and experimentally measured (dashed) test flow pitot pressure traces for the approximately tailored case.

since no allowance has been made for either circumferential variations or turbulent diffusion in the contact surface. Despite the differences attributable to structural coherence in the simulations, it should still be possible to learn something about the relevant contamination mechanisms because the flow stagnation temperature results provide independent evidence that the time of contamination is accurately simulated, at least in the over-tailored case.

4. Over-Tailored Mode Interaction

Figure 7 shows a sequence of the interaction of the reflected shock with the incident contact surface for the over-tailored case (Nitrogen driving Nitrogen). Numerical Schlieren images are shown in the upper half of the frames and mass-fractions are shown in the lower half of the frames (with driver gas in blue and driven gas in yellow). The times associated with each frame are relative to the time at which the primary diaphragm rupture process was initiated.

The first frame in Figure 7 (at 4600 μs) shows the incident contact surface and the bifurcated reflected shock. The structure of the shock reflected from the nozzle contraction assumes the form shown in Figure 7 within a distance of about one tube radius upstream of the contraction (Goozée, 2003).[1]

[1] Animations showing the flow development during diaphragm rupture and the reflected shock interactions can be accessed via http://www.mech.uq.edu.au/cfcfd/

The diaphragm rupture model has a strong influence on the contact surface shape and its evolution along the shock tube. When an instantaneously-removed diaphragm model is used in the simulations, the contact surface appears stable because it is essentially planar across the inviscid region of the shock tube diameter (Goozée, 2003). Rayleigh-Taylor stability of the contact surface is confirmed by examining the densities and acceleration of the interface: the expanded driver gas has a higher density than the driven gas (around $3.7\,\mathrm{kg/m^3}$ as compared with $1.1\,\mathrm{kg/m^3}$), and the contact surface accelerates slightly (at about $4.8\times10^3\,\mathrm{m/s^2}$) as it moves down the shock tube. However, when the iris diaphragm rupture model is used (as was the case for Figure 7), the driver gas initially appears as an annular tongue of material penetrating the driven gas. This simulated contact surface shape differs from the conventional picture of a stable interface in that the leading edge is not on the centre line of the tube. The observed shape of the simulated contact surface has its origins in the diaphragm rupture process and the flow development downstream of the primary diaphragm station. Our simulations indicate that an oblique shock structure with a Mach disk on the centre line of the tube is established soon after diaphragm rupture (Goozée, 2003). This leads to lower flow speeds on the centre line of the tube which is consistent with previous simulations incorporating a diaphragm rupture process (Cambier et al., 1992; Petrie-Repar, 2000).

As the reflected shock moves back upstream, the boundary layer does not have enough momentum to cross the normal shock, and instead boundary layer material builds up at the foot of the shock and is carried with it. This causes the flow to separate, and the shock to bifurcate into a lambda structure (Mark, 1957). The reflected shock-contact surface interaction begins at approximately $4700\,\mu$s, between the first and second frames presented in Figure 7. In these frames it is clear that a series of vortices is produced in the test gas boundary layer by the bifurcated foot of the reflected shock, prior to the reflected shock-contact surface interaction.

It is difficult to draw definite conclusions regarding the strength of the bifurcated shock relative to that observed in other works because different visualisation techniques that have been used. Furthermore, in the numerical Schlieren algorithm we have used, the density gradients have been normalised by the instantaneous maximum density gradient in each frame so as to avoid image saturation. Thus temporal variations in the grey-scale of particular features may not give reliable quantitative information.

The driver gas predominantly moves through the oblique shocks near the shock tube walls ($4800\,\mu$s frame). Vorticity is generated at the contact surface during its interaction with the reflected shock due to the baroclinic torque resulting from the misalignment of the pressure and density gradients. By the frame at $5000\,\mu$s, the driver gas at the head of the contact surface has moved towards the shock tube wall. Some driver gas is entrained into the test gas vortex structures, but significantly, a large fraction is driven back away from the shock tube walls and towards the nozzle (frames 5200 and $5400\,\mu$s). A vortex is seen to separate from the head of the driver gas structure near the shock tube centreline (frames 5600 and $5800\,\mu$s), and the contaminating driver gas accelerates along the centreline of the shock tube and into the nozzle throat (frames 6000 and $6200\,\mu$s). This mechanism causes the driver gas to arrive in the test flow prematurely here and is possibly the mechanism that causes driver gas to arrive prematurely in the test flow for over-tailored conditions in other facilities (Sudani et al., 2000).

It is important to note that the length to diameter aspect ratio of the compressed slug of test gas in this work is substantially larger than for typical (higher enthalpy) experiments in other facilities. The length of the compressed slug of test gas may affect the relative significance of the 'vortex' and 'wall-jetting' mechanisms because when the driver gas interface is closer to the end of the shock tube, jetting of the driver gas may reach the end of the shock tube before the vortices have time to develop.

5. Tailored Mode Interaction

Figures 8 and 9 show the interaction of the reflected shock with the incident contact surface for the approximately tailored case (Helium driving Nitrogen). Numerical Schlieren images are shown in the upper half of the frames and mass fractions are shown in the lower half of the frames (with the Helium driver gas in blue and the Nitrogen driven gas in yellow). The times associated with each frame are relative to the time at which the primary diaphragm rupture process was initiated.

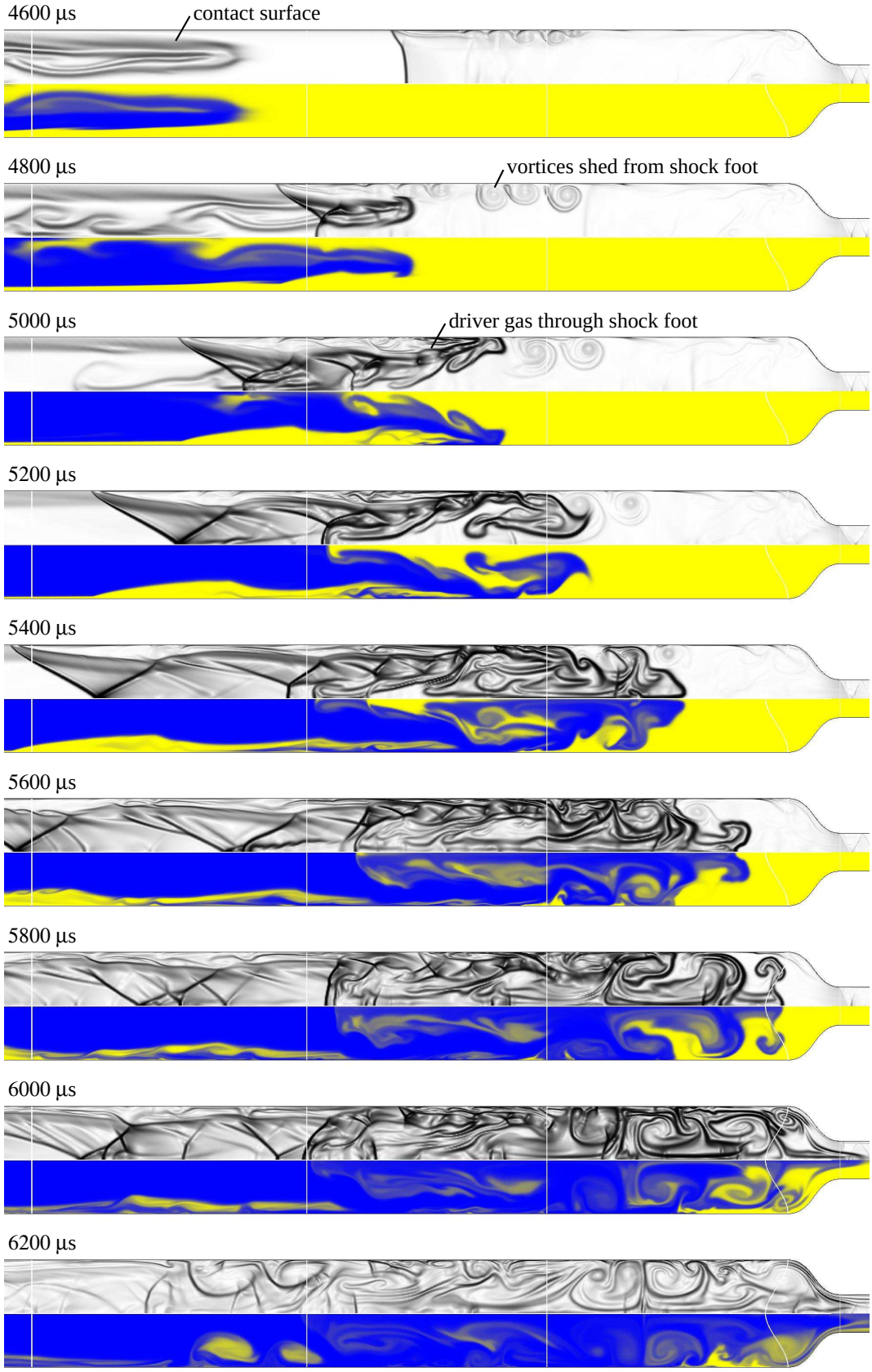

Figure 7. Sequence of numerical Schlieren images (top) and Driver gas mass fractions (bottom) showing the over-tailored interaction of the reflected shock with the contact surface and the subsequent contamination process.

The first frame, at 3100 μs, shows the incident contact surface and the reflected shock at the starting instant of their interaction. As with the over-tailored case, the diaphragm rupture model has a strong influence on the contact surface shape and its evolution along the shock tube (Goozée, 2003). However in this case, the simulations indicate that the contact surface is unstable: a distorted interface is obtained even when an instantaneously-removed diaphragm is used; the expanded driver gas has a density of around 2.5 kg/m^3, the compressed driven gas has a density of around 2.9 kg/m^3, and the contact surface accelerates along the shock tube at about 35×10^3 m/s^2. (Note that although the simulations indicate that this operating condition is slightly under-tailored – the density is lower in the driver gas by about 10 % – we have chosen to call it 'approximately tailored' because there is no clear evidence of expansion waves arising from under-tailored operation in the nozzle supply pressure history, Figure 5.)

In contrast with the over-tailored case, multiple discrete vortices are not apparent in the driven gas; only a single vortex appears to be produced in the driven gas boundary layer prior to the reflected shock-contact surface interaction. This vortex structure (most clearly seen in frame 3200 μs) continues to develop over later frames and propagates along the shock tube ahead of the driver gas. A number of vortex structures are generated in the driver gas boundary layer as the bifurcated reflected shock moves upstream (frames 3280 to 3440 μs). The motion caused by this vorticity is in a direction as to stop the jetting generated by the shock foot, as similarly observed by Chue and Itoh (1995); Chue and Eitelberg (1998). This is a tailored contact surface interaction and thus the bulk of the driver gas does not continue to move downstream immediately following interaction with the reflected shock. However, contamination is effected by vortex structures breaking away from the bulk of the driver gas and propagating downstream through the nozzle.

Figure 10 completes the description of the contamination process in the approximately tailored case by showing a sequence of driver gas mass fraction frames for later times in the end of the shock tube, the Mach 4 nozzle and the test section. The large vortex structure identified in frames 3440 to 3560 μs of Figure 9 is the main contaminating vortex that separates from the bulk of the driver gas in frames 3720 to 3880 μs of Figure 10.

As was the case with the over-tailored simulations, contamination is produced by vortical structures that propagate downstream away from the shock tube walls. These structures then accelerate through the centreline of the nozzle, contaminating the core test flow. There remains a significant portion of largely uncontaminated test gas in the shock tube after the initial contaminating structure is swept through the nozzle (frame 4520 μs).

6. Conclusions

The premature contamination of shock tube test gas with the driver gas is a ubiquitous problem that limits the practical operating envelope of shock tunnels to enthalpies (or test times) well below theoretical limits predicted by analytical techniques. Progress towards understanding shock tunnels flows and in particular, the problem of contamination, can be achieved through numerical simulation with supporting experiments. A complete shock tunnel facility has been simulated using an axisymmetric Navier-Stokes solver to avoid restrictive assumptions associated with simulating only part of a facility. Two operating conditions have been considered: one over-tailored the other approximately tailored.

By incorporating an iris-based model for the opening process of the primary diaphragm and a turbulent boundary layer on the shock tube wall, we have achieved agreement (typically to within a few percent) between the simulated and experimentally measured pressure levels behind the incident and reflected shocks. The simulated shock speeds and the rates of pressure change associated with either the tailoring waves or the reflected driver gas expansion fan are likewise simulated with sufficient accuracy to further support the conclusion that the simulations are capturing the essential fluid mechanics.

There is some discrepancy between the simulated and experimental pressure histories associated with the transit of the bifurcated reflected shock past the shock tube pressure transducer: the simulated pressure rise takes place through a sequence of discrete jumps that are not observed experimentally. Such differences have been noted in other axisymmetric shock tube simulations (Wilson, 1995). A similar sequence of discrete pressure waves is simulated in the over-tailored case through the interaction of the reflected shock and

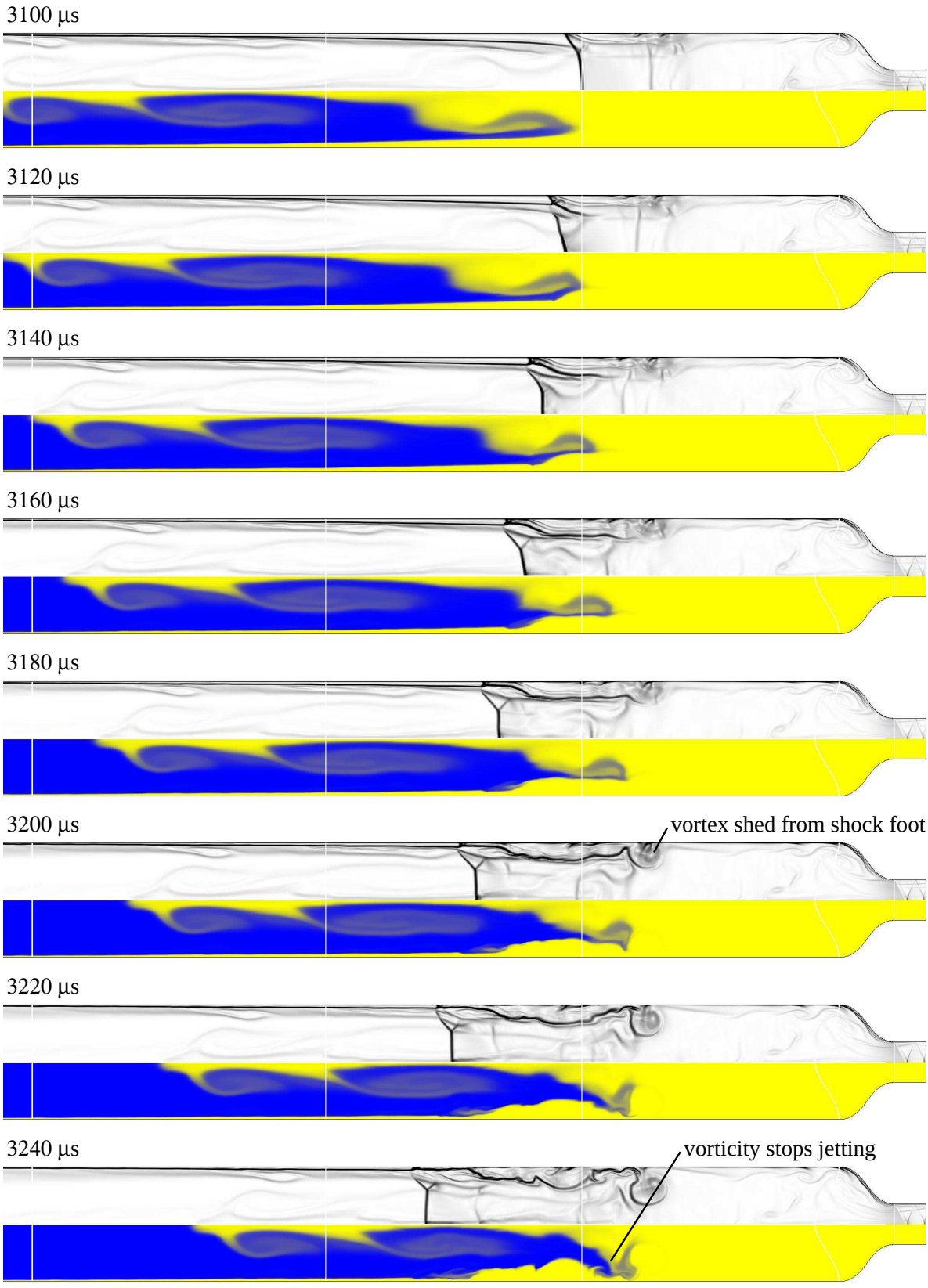

Figure 8. Part one of the sequence of numerical Schlieren images (top) and driver gas mass fractions (bottom) showing the approximately tailored interaction of the reflected shock with the contact surface. The frames start at 3.10 ms and are at 20 μs intervals.

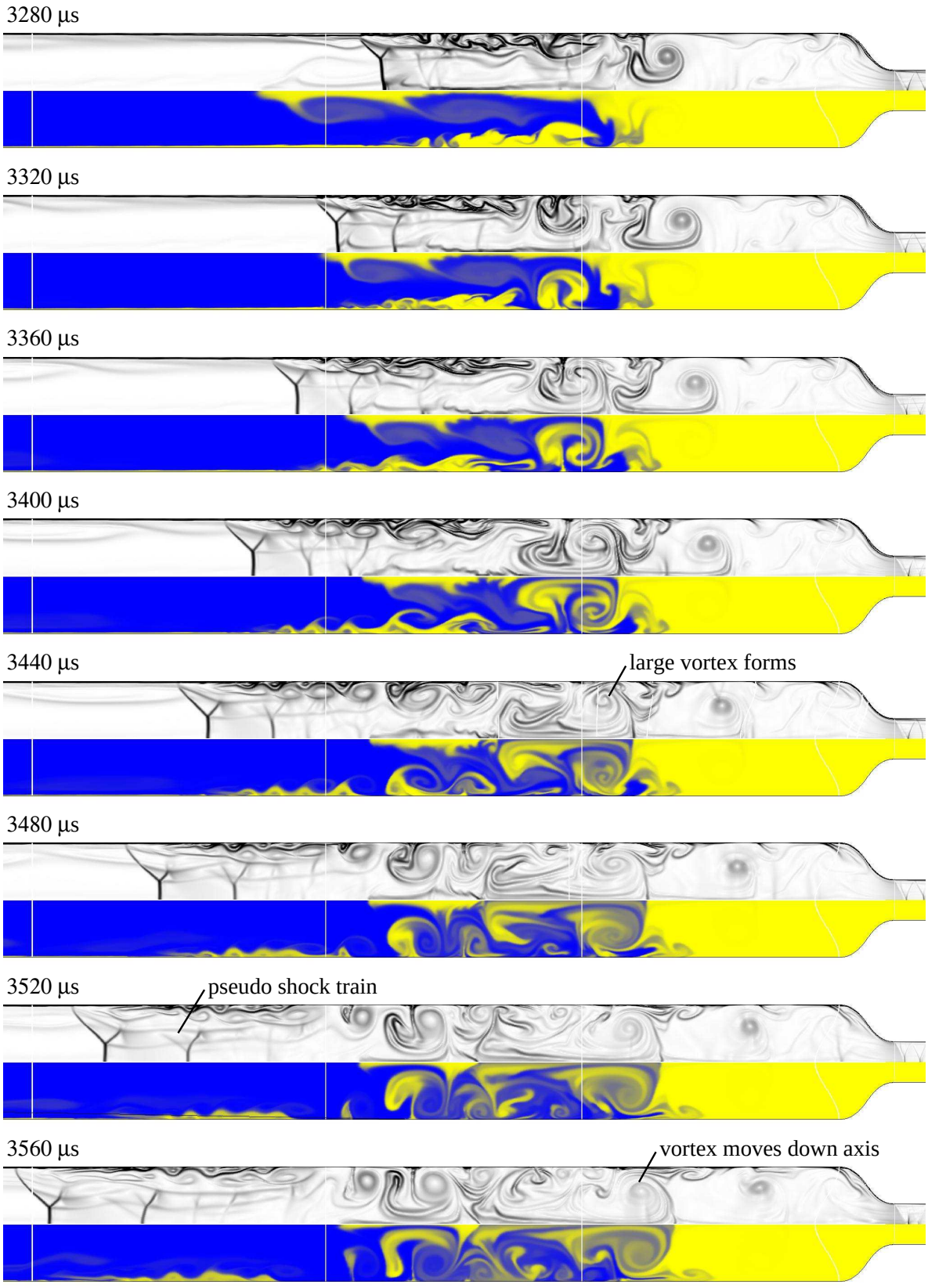

Figure 9. Part two of the sequence of numerical Schlieren images (top) and driver gas mass fractions (bottom) showing the approximately tailored interaction of the reflected shock with the contact surface. The frames start at 3.28 ms and are at 40 μs intervals.

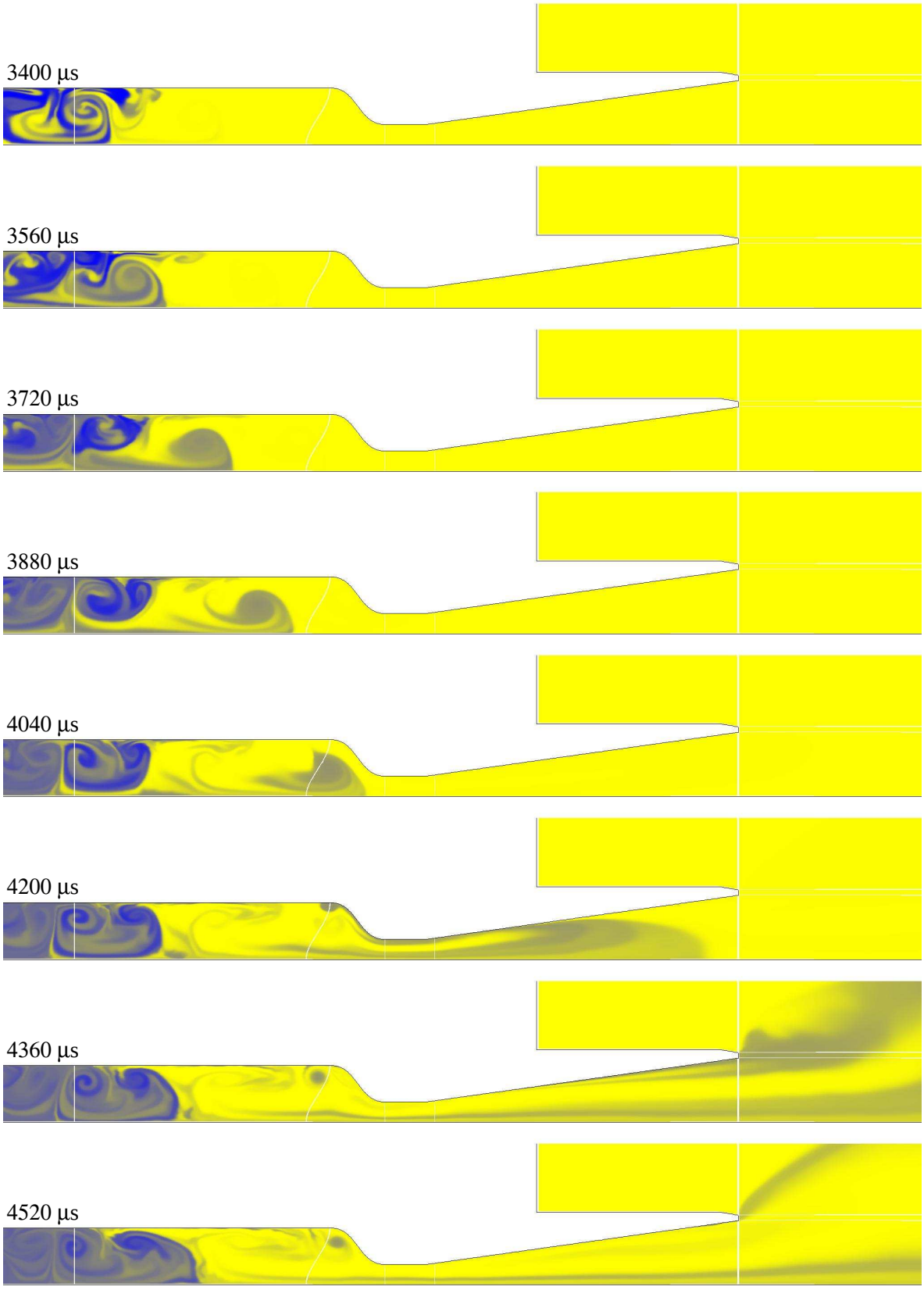

Figure 10. Sequence of driver gas mass fractions showing the contamination of the test flow with driver gas in the approximately tailored case. The driver gas in shown in blue and the test gas is shown in yellow.

the contact surface; again, such discrete pressure changes are not observed experimentally. These effects are attributed to the artificially high levels of structural coherence that are being enforced by the axisymmetric simulations and the absence of turbulent mixing at the contact surface.

Even though these limitations will have some influence on the simulation of contamination, we submit that useful information on the relevant mechanisms can still be derived from the simulations. Support for this contention is drawn from the simulation of nozzle exit stagnation temperature data in which the time of contamination is correctly simulated to within 0.1 ms, corresponding to an error in position of the contaminating structure's leading edge of less than one quarter of the tube diameter.

The simulations indicate that the bifurcated foot of the reflected shock, resulting from the interaction of the reflected shock with the boundary layer, does cause some jetting of gas as the reflected shock moves through the test gas. However, sustained jetting leading to test flow contamination is not observed because the vortices generated in the driven gas as it passes through the shock structure act to impede the jetting process. In the over-tailored case, additional vorticity of the same sign is generated at the interaction of the reflected shock and contact surface, and this similarly impedes the jetting process.

In the over-tailored case, vortices generated in the driven (test) gas boundary layer combine with the vorticity deposited at the contact surface during its interaction with the reflected shock to push driver gas away from the shock tube wall. The driver gas is then convected along the nozzle centreline, completing the contamination process. In the approximately tailored case, the interaction of reflected shock and contact surface makes little contribution to the generation of vorticity (since the driver and driven gas densities are almost matched). However, the vortices generated in the shock tube boundary layer produce a similar contamination mechanism to that observed in the over-tailored case – they project driver gas away from the wall and towards the nozzle. In the approximately tailored case, a substantial fraction of test gas remains in the shock tube after the contaminating driver gas structure first appears at the nozzle exit.

Attempting to extend the duration of the test flow through the addition of an annular gas-bleed arrangement in the shock tube (as has been done previously, for example by Sudani et al. (2000)) is unlikely to be successful at these conditions because the contaminating structures appear to be convected into the nozzle along the tube centreline. A particle trap arrangement on the shock tube centreline was investigated by Chue and Eitelberg (1998). Modification of such a device to incorporate a gas bleed has better prospects for delaying contamination at the conditions we have studied.

Acknowledgements

Richard Goozée was supported by an Australian Postgraduate Award. Computing infrastructure was provided by the Queensland Parallel Supercomputing Foundation and the Australian Partnership for Advanced Computing.

References

J. M. Austin, P. A. Jacobs, M. C. Kong, P. Barker, B. N. Littleton, and R. Gammie. The small shock tunnel facility at UQ. Department of Mechanical Engineering Report 2/1997, The University of Queensland, Brisbane, July 1997.

K. J. Badcock. A numerical simulation of boundary layer effects in a shock tube. *International Journal for Numerical Methods in Fluids*, 14:1151–1171, 1992.

B. S. Baldwin and H. Lomax. Thin layer approximation and algebraic model for separated turbulent flows. In *AIAA 16th Aerospace Sciences Meeting*, Huntsville, Alabama, 1978. AIAA Paper 78-257.

Y. Burtschell, M. Cardoso, and D. E. Zeitoun. Numerical analysis of reducing driver gas contamination in impulse shock tunnels. *AIAA Journal*, 39(12):2357–2365, 2001.

D. R. Buttsworth and P. A. Jacobs. Total temperature measurements in a shock tunnel facility. In M. C. Thompson and K. Hourigan, editors, *13th Australasian Fluid Mechanics Conference*, pages 51–54, Melbourne, December 1998.

J. L. Cambier, S. Tokarcik, and D. K. Prabhu. Numerical simulations of unsteady flow in a hypersonic shock tunnel facility. In *AIAA 17th Aerospace ground testing conference*, pages 127–140, Nashville, TN, July 1992.

M. Cardoso, Y. Burtschell, D. Zeitoun, and R. Abgrall. Numerical simulation of different methods for avoiding driver gas contamination in shock tunnels. In *Proceedings of the 21st International Symposium on Shock Waves, Volume 1*, pages 537–542, Great Keppel, Australia, 1997. Panther Publishing.

R. S. M. Chue and G. Eitelberg. Studies of the transient flows in high enthalpy shock tunnels. *Experiments in Fluids*, 25:474–486, 1998.

R. S. M. Chue and K. Itoh. Numerical analysis of reflected shock/boundary layer interaction in a high enthalpy shock tunnel. In *Proceedings of the 20th International Symposium on Shock Waves*, California Institute of Technology, Pasadena, California, 1995. World Scientific Publishing.

C. S. Craddock, P. A. Jacobs, and R. Gammie. Operational instructions for the small shock tunnel at UQ. Department of Mechanical Engineering Report 8/1998, The University of Queensland, Brisbane, July 1998.

R. J. Goozée. *Simulation of a complete shock tunnel with parallel computer codes*. PhD thesis, The University of Queensland, Brisbane, Queensland, Australia, 2003.

S. Gordon and B. J. McBride. Computer program for calculation of complex chemical equilibrium compositions and applications I. Analysis. Reference Publication 1311, NASA, October 1994.

P. A. Jacobs. MB_CNS: A computer program for the simulation of transient compressible flows. Department of Mechanical Engineering Report 10/1996, The University of Queensland, Brisbane, October 1996.

M. N. Macrossan. The equilibrium flux method for the calculation of flows with non-equilibrium chemical reactions. *Journal of Computational Physics*, 80(1):204–231, 1989.

H. Mark. The interaction of a reflected shock wave with the boundary layer in a shock tube. *Journal of the Aeronautical Sciences*, April:304–306, 1957.

B. J. McBride and S. Gordon. Computer program for calculation of complex chemical equilibrium compositions and applications II. Users manual and program description. Reference Publication 1311, NASA, June 1996.

A. Paull. A simple shock tunnel driver gas detector. *Shock Waves*, 6(5):309–312, 1996.

P. J. Petrie-Repar. *Numerical simulation of diaphragm rupture*. PhD thesis, The University of Queensland, Brisbane, Queensland, Australia, 2000.

E. M. Rothkopf and W. Low. Diaphragm opening process in shock tubes. *The Physics of Fluids*, 17(6):1169–1173, 1974.

S. P. Sharma and G. J. Wilson. Test times in hypersonic shock tubes. In *AIAA 33rd Aerospace Sciences Meeting and Exhibit*, Reno, Nevada, 1995. AIAA Paper 95-0713.

K. A. Skinner. *Mass spectrometry in shock tunnel experiments of hypersonic combustion*. PhD thesis, The University of Queensland, Brisbane, Queensland, Australia, 1994.

R. J. Stalker and K. C. A. Crane. Driver gas contamination in a high-enthalpy reflected shock tunnel. *AIAA Journal*, 16:277–278, 1978.

N. Sudani, B. Valiferdowsi, and H. G. Hornung. Test time increase by delaying driver gas contamination for reflected shock tunnels. *AIAA Journal*, 38(9):1497–1503, 2000.

Y. Wada and M. S. Liou. A flux splitting scheme with high-resolution and robustness for discontinuities. In *AIAA 32nd Aerospace Sciences Meeting*, Reno, NV, 1994. AIAA Paper 94-0083.

Y. S. Weber, E. S. Oran, J. P. Boris, and J. D. Anderson Jr. The numerical simulation of shock bifurcation near the end wall of a shock tube. *Physics of Fluids*, 7:2475–2488, 1995.

G. J. Wilson. Numerical studies of high-enthalpy impulse facilities. In *Proceedings of the 20th International Symposium on Shock Waves (Volume 1)*, California Institute of Technology, Pasadena, California, 1995. World Scientific Publishing Co. Pty. Ltd.